

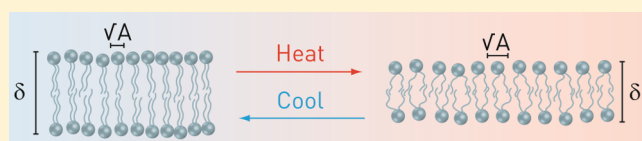
Effect of Temperature on the Structure of Charged Membranes

Pablo Szekely,^{†,‡} Tom Dvir,^{†,‡} Roi Asor,[†] Roi Resh,^{†,‡} Ariel Steiner,[†] Or Szekely,[†] Avi Ginsburg,^{†,§} Jonathan Mosenkis,[†] Vicky Guralnick,[†] Yoav Dan,[†] Tamar Wolf,[†] Carmen Tamburu,[†] and Uri Raviv^{*,†}

[†]The Institute of Chemistry, [‡]The Racah Institute of Physics, [§]School of Pharmacy, The Hebrew University of Jerusalem, Edmond J. Safra Campus, Givat Ram, 91904 Jerusalem, Israel

S Supporting Information

ABSTRACT: Interactions between charged and neutral self-assembled phospholipid membranes are well understood and take into account temperature dependence. Yet, the manner in which the structure of the membrane is affected by temperature was hardly studied. Here we study the effect of temperature on the thickness, area per lipid, and volume per lipid of charged membranes. Two types of membranes were studied: membranes composed of charged lipids and dipolar (neutral) membranes that adsorbed divalent cations and became charged. Small-angle X-ray scattering data demonstrate that the thickness of charged membranes decreases with temperature. Wide-angle X-ray scattering data show that the area per headgroup increases with temperature. Intrinsically charged membranes linearly thin with temperature, whereas neutral membranes that adsorb divalent ions and become charged show an exponential decrease of their thickness. The data indicate that, on average, the tails shorten as the temperature rises. We attribute this behavior to higher lipid tail entropy and to the weaker electrostatic screening of the charged headgroups, by their counterions, at elevated temperatures. The latter effect leads to stronger electrostatic repulsion between the charged headgroups that increases the area per headgroup and decreases the bilayer thickness.



INTRODUCTION

Phospholipids spontaneously self-assemble in water into bilayers that form flat membranes or vesicles that resemble biological membranes. Neutral lipids containing the phosphatidylcholine (PC) headgroup self-assemble into multilamellar structures that have been well studied.^{1–4} For most lipid types, both structural data^{4–6} and thermodynamic data⁷ are available. Charged membranes were less studied as they strongly repel one another and separate, in water, to large distances relative to their thickness, δ ,⁸ and are harder to orient,⁹ hence it is more difficult to study their structure.

Most of the published structural data do not take the temperature dependence of the membrane thickness into account. Usually⁴ the membrane thicknesses are assumed to be constant or with a negligible variance, with respect to temperature. The entire difference in the measured distance under different temperatures is attributed to the variation in the water layer thickness between the membranes. This assumption may lead to errors when investigating the nature of strong attractions between membranes, where the typical water layer thickness is of the same order of magnitude as the membrane thickness. It is also important when trying to characterize the maximum swelling distance of charged membranes,^{10,11} as the swelling distance linearly depends on the thickness of the membranes.

In this study, we describe how temperature controls the thickness and area per headgroup of charged membranes. We studied two types of charged membranes. Intrinsically charged lipids containing the sn-glycero-3-phospho-L-serine (PS) headgroup and induced charged membranes. The latter was obtained by charging

neutral membranes containing the PC headgroup by adding divalent cations to the solution. If the tails of the lipids are saturated, the divalent ions can adsorb and charge the dipolar headgroups.^{12–15} We show how the membrane structure varies with temperature and offer a possible qualitative explanation for the observations that may serve as a basis for a more rigorous theory.

MATERIALS AND METHODS

Two anionic lipids were used: dilauroyl ($C_{12:0}$) and dioleoyl ($C_{18:1}$) sn-glycero-3-phospho-L-serine (DLPS and DOPS, respectively). The neutral 1,2-dilauroyl ($C_{12:0}$) sn-glycero-3-phosphocholine (DLPC) lipid was also used. The lyophilized lipid powders were used as received from Avanti Polar Lipids, Inc., AL. The chemical structure of those lipids is shown in Sketch S1 of the Supporting Information (SI, section 3). We added highly purified water¹⁶ (Barnstead Nanopure Diamond) to each of the lyophilized pure PS lipids to obtain lipid solutions at the required final lipid volume fractions, ϕ . In the case of DLPC, we prepared a 5 or 10 mM solutions of $CaCl_2$ and mixed them with the lyophilized lipid powder. Each lipid solution was vortex mixed for ca. 1 h, above the lipid melting temperature, in a glass vial. The solution was then transferred into a quartz capillary that was flame sealed and centrifuged at a relative centrifugal force (RCF) of 6000g, using a SIGMA 1-15PK centrifuge equipped with rotor No. 11024, suitable for capillaries.

Received: August 7, 2011

Revised: October 10, 2011

Published: October 11, 2011

Using our in-house high-resolution solution small-angle and wide-angle X-ray scattering (SAXS and WAXS) setup, described earlier,^{15,17–19} we determined the electron density profile of the bilayers and hence their head-to-head distance, δ_{hh} , the area per headgroup, and the repeat distance, D , of the lamellar phases. The measurements were performed in a temperature-controlled sample chamber (Forvis Technologies Inc., CA) with 0.01 °C accuracy. After we changed the temperature, we waited for ca. 90 min to let the lipid solution equilibrate at the new temperature (for details see SI, section 1 and Figure S1).

In our in-house setup the X-ray generator, MicroMax-007HF (Rigaku Corporation), is a rotating anode, running at 40 kV and 30 mA, and has a copper target producing K_{α} photons with energy of 8 keV (wavelength of 1.54 Å). The rotating anode is water chilled by a refrigerated air-cooled system (Haskris, R075). The focal spot size on the anode is $70 \times 70 \mu\text{m}^2$. A focused monochromatic beam is obtained using Confocal Max-Flux optics, CMF-12-100Cu8 focusing unit (Osmic Inc., a Rigaku Company). The beam continues into a vacuumed flight-path (ca. 15 Torr), 1 in. in diameter containing two slits. The slits are fully motorized scatterless²⁰ hybrid metal–Ge single-crystal slits (Forvis Technologies, Inc.). Performance is optimized when the first slit (after the optics) is set to $1 \times 1 \text{ mm}^2$ and the beam spot size is set by the second slit (close to the sample) at $0.7 \times 0.7 \text{ mm}^2$. Our motorized sample stage consists of a Huber goniometer (for controlling the rotation angle), combined with X–Y–Z translation stages (Forvis Technologies, Inc.). The scattered beam enters a large He-filled flight path (ca. 36 cm in diameter), enabling a sample-to-detector distance of ca. 1.84 m. A MAR345 image-plate detector (Marresearch GmbH) is located at the end of the flight path on a motorized plate. For solution WAXS measurements, we removed the He-filled flight path and moved the detector as close as possible to the sample (sample-to-detector of ca. 23 cm). A more detailed description of our setup was given elsewhere.¹⁹

Some of the data were taken in the 5.2 L beamline at the ELETTRA synchrotron (Trieste, Italy) described earlier.¹⁷ In this setup, the X-ray photon energy was 8 keV; Si₁₁₁ was used as a monochromator; the beam size was set to $1000 \times 500 \mu\text{m}^2$ (H and V full width at half maximum, respectively); and an image plate detector MAR300 (Marresearch GmbH, Germany) was used.

Full analysis of both the form factor and the structure factor of the radially integrated scattering curves, using the analysis software, X+,¹⁸ yielded the structural parameters mentioned above. We used a model of a stack of infinite flat slabs having a Gaussian electron density profile, along the z direction that is normal to the membrane plane, as described.¹⁷ The use of three Gaussians as a model for the electron density of a lipid bilayer is an approximation to the actual electron density distribution, though it has been showed that the Gaussian profile produces good fits in the case of lipid bilayers.^{3,17,21} The quality of the data and the measured q -range (where q is the magnitude of the momentum transfer vector) are important factors that could introduce inaccuracies in the fitting of the models, as those are inherently over parametrized.¹⁷ In our case, the quality of the data and q -range are sufficient to well estimate the thickness of the membrane.

Interfaces composed of self-assembled molecules such as lipid membranes are characterized by a correlation length, known as the persistence length, ξ , beyond which the orientations of distant points on the membrane become uncorrelated.

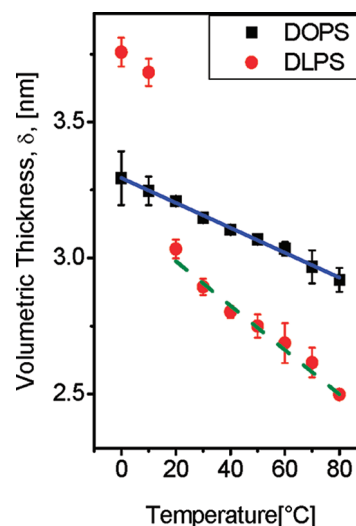


Figure 1. Volumetric membrane thickness, δ , of DOPS (squares) and DLPS (circles) as a function of temperature. Each lipid fits to a linear temperature relation: $\delta = a(T - 273) + b$. For DOPS, $a = (-4.6 \pm 0.2) \times 10^{-3} \text{ nm/}^\circ\text{C}$ and $b = 3.295 \pm 0.007 \text{ nm}$; for DLPS $a = (-8.2 \pm 0.2) \times 10^{-3} \text{ nm/}^\circ\text{C}$ and $b = 3.15 \pm 0.02 \text{ nm}$. Note that DLPS has a phase transition at ca. 18 °C (Figure S2, SI), below which the DLPS membranes are in a lamellar liquid crystalline phase L_{β} (gel phase), and above it, the membranes become liquid. For DLPS, only the data in the liquid phase are taken into account for the linear fit.

ξ is given by^{22–24}

$$\xi = a_m \exp(4\pi\kappa/3k_B T) \quad (1)$$

where a_m is the molecular size (of order few Å); κ is the membrane bending rigidity; k_B is the Boltzmann constant; and T is the temperature. The charged membranes used in this study are rigid,²⁵ and their ξ is very large (ca. 10^8 m or longer). In pure water, the electrostatic repulsion between the charged bilayers and their large ξ should lead to an ideally swelling lamellar phase with a repeat distance^{8,10,25,26} given by

$$D_{\text{ideal}} = \delta/\phi \quad (2)$$

D_{ideal} is the ideal-swelling repeat lamellar distance; δ is the membrane thickness; and ϕ is the lipid volume fraction.

To measure the thickness of the membranes, we prepared lipid solutions with different volume fractions, for two different analysis methods. For solution with high lipid volume fractions (~ 0.2 or higher), the structure factor dominates, and the ideal-swelling relation holds and was used to determine the membrane thickness.¹⁰ This method is also called the volumetric method for finding the volumetric membrane thickness, δ . In dilute lipid solutions, the form factor dominated the scattering signal and enabled us to fit the data to a model of Gaussian electron density profiles and extract the head-to-head distance, δ_{hh} .¹⁸

RESULTS AND DISCUSSION

Using solution SAXS, we measured the scattering signal of different lipid concentrations at varying temperatures. The signals were radially integrated, and the scattering intensity, I , was plotted as a function of the magnitude of the momentum transfer vector, q (Figures S5 and S6, SI). The membrane thicknesses were deduced from those scattering profiles. At high concentrations, the structure-factor dominates the signal, and the

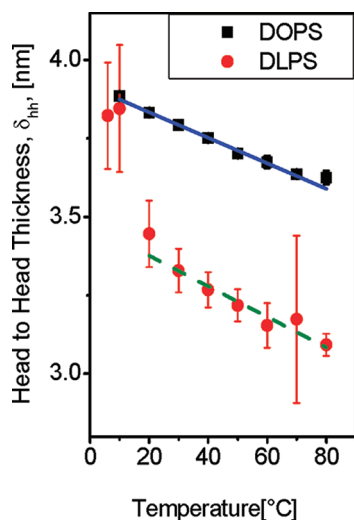


Figure 2. Head-to-head thickness, δ_{hh} , of DOPS (squares) and DLPS (circles) obtained from the electron density profile of the membranes as a function of temperature. δ_{hh} of each lipid follows a linear relation: $\delta_{hh} = a(T - 273) + b$. For DOPS, $a = (-3.8 \pm 0.2) \times 10^{-3}$ nm/degree and $b = 3.91 \pm 0.01$ nm; for DLPS $a = (-4.9 \pm 0.4) \times 10^{-3}$ nm/degree and $b = 3.47 \pm 0.03$ nm. The reservations mentioned in Figure 1 apply here as well.

volumetric thickness is easily obtained by finding the repeat distance of the lamellar phases (Figure S5, SI) and using the ideal-swelling relation (eq 2). At low concentrations, the form factor dominates the signal, and using the program X+,¹⁸ we could fit an electron density profile model and extract the relevant structural parameters. All the results presented in this paper correspond to the mean values and the statistical variance of several repeated measurements. Repeated heating and cooling cycles verified the reversibility of the results, hence the equilibrium of the studied lipid solutions.

Our results indicate that the volumetric thickness of charged membranes, composed of DOPS or DLPS, linearly decreases with the temperature (Figure 1). In the measured temperature range, DOPS membranes are in the liquid phase.²⁷ DLPS has a phase transition at 18 °C²⁸ (Figure S2 in the SI, section 2) from the lamellar liquid crystalline phase L_β (or gel phase) to the liquid-disordered phase. The membrane in the gel phase is thicker than in the liquid phase by ca. 0.5 nm. In the liquid phase, both DLPS and DOPS, which have the charged PS headgroup, show a similar linear behavior. DOPS, which has a longer tail, is thicker than DLPS, as the results clearly confirm.

The head-to-head distance, δ_{hh} , behaves qualitatively in a similar manner as the volumetric thickness, δ , but is systematically larger (Figure 2). The phase transition of DLPS, the ratio between both lipids and the linear descent of the thickness, appear in $\delta_{hh}(T)$ as in $\delta(T)$. We could naïvely expect δ to be larger than δ_{hh} , since the former is an average thickness of the entire bilayer, whereas the latter describes the thickness from one phosphate moiety to its opposing counterpart, without taking into account the contributions of the phosphates' residues that may extend beyond the phosphate groups themselves (SI, section 3 and Sketch S1). Comparison between both thicknesses demonstrates the opposite relation, though the ratio between the thicknesses weakly depends on temperature and lipid type (Figure S3 and SI, section 4). The ratio between both thicknesses measured concurs with an earlier ratio between two similar means to estimate membrane thicknesses.²⁹

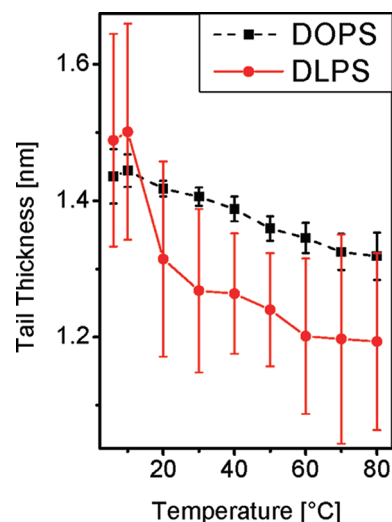


Figure 3. Tail thickness of DOPS (squares) and DLPS (circles) obtained from the membrane's electron density profiles as a function of temperature (see for example Figure S6, SI). The tails account for most of the decrease in the membrane thickness. The phase transition of DLPS at 18 °C is noticeable (see also Figure S2, SI).

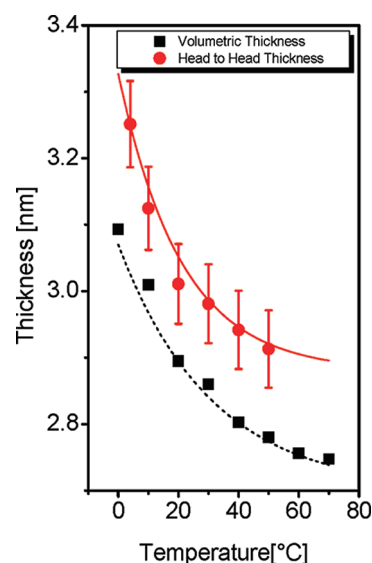


Figure 4. Volumetric thickness (squares) of DLPC ($\phi = 0.24$) with 10 mM CaCl_2 and the head-to-head thickness (spheres) of DLPC ($\phi = 0.014$) with 10 mM CaCl_2 are plotted as a function of temperature. The broken curves are qualitative fits to exponential decay functions of the form $A \times \exp\{-(T - 273)/B\} + C$ where $A = 0.447$, $B = 20.9$, and $C = 2.88$ for the head-to-head thickness (solid curve) and $A = 0.37$, $B = 31$, and $C = 2.7$ for the volumetric thickness (broken curve).

The decrease in the thickness of the membranes results from a decrease in their tail thickness. Further analysis of the electron density profile suggests that the major contributor to the decrease in the head-to-head distance is the position of the head's Gaussian center with respect to the tail's Gaussian center. Pabst and Nagle^{21,30} defined the tail length as the difference between this length and half of the head's Gaussian width, meaning that the difference between Gaussian's center positions can be attributed to the tail's length if the head's Gaussian thickness remains constant (Figure 3).

The volumetric thickness of neutral (zwitterionic) membranes charged by divalent ions decreases in a similar manner to that of membranes with PS headgroups (Figure 4). This observation suggests that the decrease of the membrane thickness is not headgroup specific. We prepared a solution of charged membranes by adding Ca^{2+} ions to DLPC. The Ca^{2+} ions bind to the membrane and charge its surface.^{15,31}

While the thickness of intrinsically charged membranes decays linearly, the thickness of calcium-induced charged membranes decays exponentially. An earlier study shows that at ambient room temperature the addition of Ca^{2+} does not significantly affect the thickness of the DLPC membrane.¹⁵

The SAXS data of the phospholipid membranes clearly demonstrate that the thickness of a charged membrane decreases upon heating. Both δ_{hh} and δ of intrinsically charged membranes linearly thin with temperature. The thickness of calcium-induced charged membranes exponentially decays with the temperature. The data indicate that, on average, the tails get shorter as the temperature rises and play a major factor in the change of the membrane thickness.

In neutral membranes, a certain decrease in the tail length was observed in earlier studies: an NMR study³² showed that the chain length decreases with temperature, and in parallel, the area per headgroup increases. A variety of saturated zwitterionic lipid bilayers (DLPC, DMPC, DPPC, DSPC, and DPPE) behave in a similar way. Yet, there are too few data points per lipid available. A small-angle neutron scattering (SANS) study³³ demonstrated that the thickness of saturated zwitterionic lipid bilayers (DPPC and DMPC) decreases with temperature.

Possibly, the difference between the head-to-head distance and the volumetric thickness originates mainly from small deviations from ideal-swelling behavior. This ideal behavior assumes that a single lamellar phase fills out the entire volume and that all the water molecules in the system fill the gap between membranes. This picture is unrealistic as the lamellar phase, which is a 1D crystal, cannot have a true long-ranged order,³⁴ and water penetrates between headgroups and becomes an essential component of the fluid lipid membrane.^{1,29} More realistically, the lipid solution is composed of finite size domains of tightly packed multilamellar vesicles with some water penetrating into the lipid membrane itself.⁴ Due to excluded voids between the multilamellar vesicles and water penetration, the effective volume available for the lipid is smaller than the total volume; hence, the effective volume fraction is higher than expected. Another possible source for the smaller volumetric thickness could be that the swelling of the lamellar phase is nonideal because an entropically driven disordered phase may coexist at those lipid concentrations.¹⁵ Therefore, the ideal-swelling relation provides a lower bound for the membrane thickness, and the head-to-head distance, δ_{hh} , is likely to better estimate the membrane thickness.

Although all of the results consistently show a decrease of the membrane thickness as the temperature raises, the DLPS thickness decrease rate appears significantly different between the two methods, while the DOPS does not show such a dramatic effect. In DLPS, which has saturated tails, the packing of the lipids within the bilayer is tighter, and less water molecules can penetrate into the bilayer. As the temperature rises, the area per headgroup increases (Figure 5), and more water molecules penetrate into the bilayer.^{1,29} In DOPS, which has unsaturated tails and looser packing, the water molecules penetrate into the bilayer already at low temperature. Therefore, the deviation from ideal-swelling behavior in DLPS will be larger than in DOPS, and the volumetric method is less accurate in the case of DLPS;

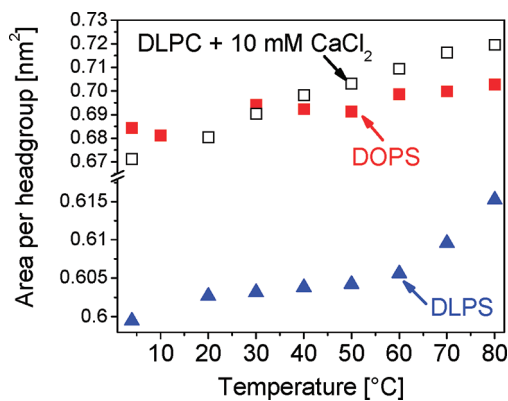


Figure 5. Area per headgroup of each lipid, obtained from wide-angle X-ray scattering measurements, as a function of temperature.

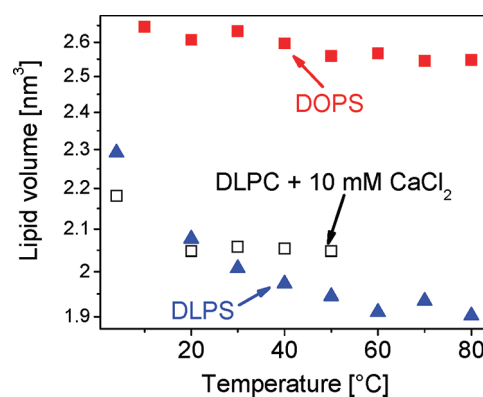


Figure 6. Volume of each lipid as a function of temperature. The lipid volumes were obtained by multiplying the head-to-head thicknesses in Figures 2 and 4 by the corresponding areas per headgroup in Figure 5.

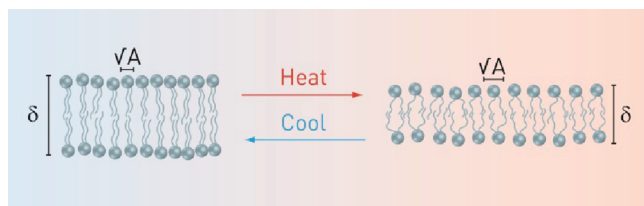
hence, its thickness appears to drop faster. The electron density profile does not rely on the ideal-swelling behavior and takes the penetration of water into account, hence the measured thickness variation rate, a , in both lipids is similar.

We attribute the decrease of charged membrane thickness to the electrostatic in-plane repulsion between the charged headgroups. At higher temperatures, the counterions of the charged headgroups have higher kinetic energy, and they extend farther away from the membrane.³⁵ The screening length increases with temperature, and the repulsion between the charged headgroups strengthens. The lipids are unlikely to significantly change their volumes in the range of temperatures used in our experiments (see later). Therefore, to compensate for the stronger lateral stress, the area per headgroup should increase. At higher temperatures, the tail entropy increases, and the tails are likely to assume wider conformations that may increase the area per headgroup.

To test this hypothesis, we performed solution WAXS measurements at different temperatures. From the center of the lipid-tail Gaussian correlation peaks, centered at q values in the range between ca. 13.5 and 15 nm^{-1} , we could estimate, as explained,^{17–19} the area per lipid headgroup in each membrane at each temperature.

Figure 5 shows that the area per headgroup of each lipid increases with temperature, hence supporting our hypothesis. Using the data in Figures 2, 4, and 5 we could obtain the mean volume per lipid in the membranes at each temperature

Scheme 1. Illustrating the Structural Changes upon Heating Charged Membranes^a



^a As the temperature increases, the counterions have higher thermal energy and on average are farther away from the membrane surface. The screening length therefore increases, and the repulsion between the headgroups increases. The entropy of the tail increases with temperature, and wider tail conformations are favorable. As a result, the mean area per headgroup, A , increases (Figure 5). Since the lipid volume does not change much in the range of temperatures used in our experiments (Figure 6), the membrane thickness decreases, to reduce the interfacial area between the aqueous solution and the lipid tails.

(Figure 6). Apart from the change around the gel-to-liquid phase transition temperature, the decrease in the membrane thickness with increasing temperature is nearly inversely proportional to the increase in the area per headgroup, as is illustrated in Scheme 1. The wider lipid tail conformation at elevated temperatures is driven by the higher tail entropy and helps to reduce the contact of the hydrophobic tails with water, when the area per lipid increases.

The thickness of the calcium-induced charged membranes decays exponentially. This membrane is more complicated because by increasing the temperature the screening length increases, but at the same time the membrane charge density may decrease due to desorption of Ca^{2+} ions above some critical temperature. This desorption overcomes the lateral electrostatic stress in the membrane, and higher temperatures lead to a weaker increase in the area per headgroup; hence, the extent of membrane thinning decreases with temperature.

CONCLUSIONS

In this paper, we presented the variation in the thickness, area per headgroup, and volume of charged membranes over a wide temperature range. There is a difference in the behavior of intrinsically charged membranes and multivalent ion-induced charged membranes. The membrane thickness thins linearly with the temperature in the former case and exponentially in the latter case. Moreover, we measured the volumetric thickness and the head-to-head distance with a SAXS setup and showed that the volumetric thickness is a lower bound to the head-to-head thickness. We also found that the decrease of the membrane thickness with temperature is accompanied by an increase in the area per headgroup. According to the Poisson–Boltzmann mean field theory,³⁵ the higher thermal energy of the counterions leads to their broader distribution away from the surface, weaker electrostatic screening of the charged headgroups, and stronger repulsion between them. We expect this repulsion together with the higher lipid-tail entropy, which should increase with temperature, to cause the observed increase in the area per headgroup. Larger area per headgroup is likely to enable conformational changes of the tails that thin the membranes

with increasing temperature, to minimize contact with the aqueous solution.

ASSOCIATED CONTENT

S Supporting Information. We (1) provide data regarding the time it takes the lipid solution to reach equilibrium, (2) show in greater detail the variation of the membrane thickness of DLPS near its gel-to-liquid phase transition, (3) show the chemical structure of the lipid used in this study, (4) show the ratio between the volumetric and head-to-head thicknesses, and (5) show a few examples of several key steps in the analysis of the SAXS data from the 2D raw images to the analyzed 1D data and model fitting. This material is available free of charge via the Internet at <http://pubs.acs.org>.

AUTHOR INFORMATION

Corresponding Author

*E-mail: raviv@chem.ch.huji.ac.il.

ACKNOWLEDGMENT

We acknowledge helpful discussions with D. Harries and P. A. Pincus. We thank H. Amenitsch and the SAXS beamline staff at Elettra, Trieste, for their support and experimental help as well as M. Bonjack and N. Ganot for their assistance. This project was supported by the Israel Science Foundation, the US-Israel Binational Science Foundation, and the James Frank program. P.S. and O.S. acknowledge support from the Samuel and Lottie Rudin Foundation fellowships. T.D. acknowledges support from a short-term fellowship of the institute of chemistry and the faculty of mathematics and sciences at the Hebrew University. U.R. acknowledges support from the Alon Fellowship for young investigators. We thank the Safra, Wolfson, and Rudin foundations for supporting our laboratory.

REFERENCES

- (1) Simon, S. A.; McIntosh, T. J. *Methods Enzymol.* **1986**, *127*, 511.
- (2) Simon, S. A.; Advani, S.; McIntosh, T. J. *Biophys. J.* **1995**, *69*, 1473.
- (3) McIntosh, T. J.; Simon, S. A. *Biochemistry* **1986**, *25*, 4058.
- (4) Nagle, J. F.; Tristram-Nagle, S. *Curr. Opin. Struct. Biol.* **2000**, *10*, 474.
- (5) Tristram-Nagle, S.; Petrache, H. I.; Nagle, J. F. *Biophys. J.* **1998**, *75*, 917.
- (6) Kucerka, N.; Liu, Y. F.; Chu, N. J.; Petrache, H. I.; Tristram-Nagle, S. T.; Nagle, J. F. *Biophys. J.* **2005**, *88*, 2626.
- (7) Petrache, H. I.; Tristram-Nagle, S.; Harries, D.; Kucerka, N.; Nagle, J. F.; Parsegian, V. A. *J. Lipid Res.* **2006**, *47*, 302.
- (8) Cowley, A. C.; Fuller, N. L.; Rand, R. P.; Parsegian, V. A. *Biochemistry* **1978**, *17*, 3163.
- (9) Tristram-Nagle, S. A. *Preparation of oriented, fully hydrated lipid samples for structure determination using X-ray scattering*; Springer: New York, 2007; Vol. 400, p 63.
- (10) Deme, B.; Dubois, M.; Gulik-Krzywicki, T.; Zemb, T. *Langmuir* **2002**, *18*, 997.
- (11) Lyonnard, S.; Bartlett, J. R.; Sizgek, E.; Finnie, K. S.; Zemb, T.; Woolfrey, J. L. *Langmuir* **2002**, *18*, 10386.
- (12) Lis, L. J.; Parsegian, V. A.; Rand, R. P. *Biochemistry* **1981**, *20*, 1761.
- (13) Lis, L. J.; Lis, W. T.; Parsegian, V. A.; Rand, R. P. *Biochemistry* **1981**, *20*, 1771.

- (14) McLaughlin, A.; Grathwohl, C.; McLaughlin, S. *Biochim. Biophys. Acta* **1978**, *513*, 338.
- (15) Szekely, O.; Steiner, A.; Szekely, P.; Amit, E.; Asor, R.; Tamburu, C.; Raviv, U. *Langmuir* **2011**, *27*, 7419.
- (16) Belitzky, A.; Melamed-Book, N.; Weiss, A.; Raviv, U. *Phys. Chem. Chem. Phys.* **2011**, *13*, 13809.
- (17) Szekely, P.; Ginsburg, A.; Ben-Nun, T.; Raviv, U. *Langmuir* **2010**, *26*, 13110.
- (18) Ben-Nun, T.; Ginsburg, A.; Szekely, P.; Raviv, U. *J. Appl. Crystallogr.* **2010**, *43*, 1522.
- (19) Nadler, M.; Steiner, A.; Dvir, T.; Szekely, O.; Szekely, P.; Ginsburg, A.; Asor, R.; Resh, R.; Tamburu, C.; Peres, M.; Raviv, U. *Soft Matter* **2011**, *7*, 1512.
- (20) Li, Y. L.; Beck, R.; Huang, T.; Choi, M. C.; Divinagrancia, M. *J. Appl. Crystallogr.* **2008**, *41*, 1134.
- (21) Nagle, J. F.; Tristram-Nagle, S. *Biochim. Biophys. Acta, Rev. Biomembr.* **2000**, *1469*, 159.
- (22) Degennes, P. G.; Taupin, C. *J. Phys. Chem.* **1982**, *86*, 2294.
- (23) Peliti, L.; Leibler, S. *Phys. Rev. Lett.* **1985**, *54*, 1690.
- (24) D. Nelson, T. P., Weinberg, S. *Statistical Mechanics of Membranes and Surfaces*, 2nd ed.; World Scientific: New Jersey, 2004.
- (25) Petrache, H. I.; Tristram-Nagle, S.; Gawrisch, K.; Harries, D.; Parsegian, V. A.; Nagle, J. F. *Biophys. J.* **2004**, *86*, 1574.
- (26) Deme, B.; Dubois, M.; Zemb, T. *Langmuir* **2002**, *18*, 1005.
- (27) Israelachvili, J. N. *Intermolecular and Surface Forces*, 2nd ed.; Academic Press: New York, 1992.
- (28) Lewis, R.; McElhaney, R. N. *Biophys. J.* **2000**, *79*, 2043.
- (29) Gordeliy, V. I.; Cherezov, V.; Teixeira, J. *Phys. Rev. E* **2005**, *72*.
- (30) Pabst, G.; Rappolt, M.; Amenitsch, H.; Laggner, P. *Phys. Rev. E* **2000**, *62*, 4000.
- (31) Marra, J.; Israelachvili, J. *Biochemistry* **1985**, *24*, 4608.
- (32) Petrache, H. I.; Dodd, S. W.; Brown, M. F. *Biophys. J.* **2000**, *79*, 3172.
- (33) Gordeliy, V. I.; Cherezov, V. G.; Teixeira, J. *J. Mol. Struct.* **1996**, *383*, 117.
- (34) Mermin, N. D.; Wagner, H. *Phys. Rev. Lett.* **1966**, *17*, 1133.
- (35) Andelman, D. Electrostatic Properties of Membranes: The Poisson–Boltzmann Theory. In *Handbook of Biological Physics*; Elsevier Science B.V.: Amsterdam, 1995; p 603.